doi:10.1016/j.jmb.2009.01.022 J. Mol. Biol. (2009) 386, 1265–1277

JMB

Available online at www.sciencedirect.com

ScienceDirect

ELSEVIER

Solution Structure of S100A1 Bound to the CapZ Peptide (TRTK12)

Nathan T. Wright[1], Brian R. Cannon[1], Paul T. Wilder[1], Michael T. Morgan[1], Kristen M. Varney[1], Danna B. Zimmer[2] and David J. Weber[1]*

[1]*Department of Biochemistry and Molecular Biology, University of Maryland School of Medicine, 108 North Greene Street, Baltimore, MD 21201, USA*

[2]*Department of Veterinary Pathobiology, College of Veterinary Medicine, Texas A&M University, College Station, TX 77843-44467, USA*

Received 10 December 2008; received in revised form 13 January 2009; accepted 15 January 2009
Available online 22 January 2009

As is typical for S100–target protein interactions, a Ca^{2+}-dependent conformational change in S100A1 is required to bind to a 12-residue peptide (TRTK12) derived from the actin-capping protein CapZ. In addition, the Ca^{2+}-binding affinity of S100A1 is found to be tightened (greater than threefold) when TRTK12 is bound. To examine the biophysical basis for these observations, we determined the solution NMR structure of TRTK12 in a complex with Ca^{2+}-loaded S100A1. When bound to S100A1, TRTK12 forms an amphipathic helix (residues N6 to S12) with several favorable hydrophobic interactions observed between W7, I10, and L11 of the peptide and a well-defined hydrophobic binding pocket in S100A1 that is only present in the Ca^{2+}-bound state. Next, the structure of S100A1–TRTK12 was compared to that of another S100A1–target complex (i.e., S100A1–RyRP12), which illustrated how the binding pocket in Ca^{2+}-S100A1 can accommodate peptide targets with varying amino acid sequences. Similarities and differences were observed when the structures of S100A1–TRTK12 and S100B–TRTK12 were compared, providing insights regarding how more than one S100 protein can interact with the same peptide target. Such comparisons, including those with other S100–target and S100–drug complexes, provide the basis for designing novel small-molecule inhibitors that could be specific for blocking one or more S100–target protein interactions.

Edited by M. F. Summers

Keywords: S100A1; target binding; CapZ; S100 proteins; NMR

Introduction

S100A1 is a dimeric Ca^{2+}-binding protein (10.5 kDa per subunit) in the S100 protein family and has two EF-hands per subunit. In the N-terminus, each S100A1 subunit has a 14-residue EF-hand (EF1; residues 19–32) termed the "S100-hand" or the "pseudo-EF-hand". EF1 typically binds Ca^{2+} weakly via several backbone carbonyl ligands and a bidentate ligand from a glutamate (E32) at position 14 of the Ca^{2+}-binding domain. In the C-terminus, each S100A1 subunit has a canonical 12-residue EF-hand (EF2; residues 62–73) that coordinates Ca^{2+} in a manner identical with that of other proteins in the EF-hand superfamily, such as calmodulin and troponin C.[1] As with most dimeric S100 proteins, only EF2 of S100A1 undergoes a large structural rearrangement upon binding Ca^{2+}, and it is this conformational change that allows S100A1 to exert its biological function via interaction with and modulation of cellular targets. This conformational change in S100A1 involves the rotation of the entering helix of EF2 (helix 3) by ~90° rather than the exiting helix (helix 4) as found for most other EF-hand-containing proteins and is the defining characteristic of an "S100 Ca^{2+} switch".[2–4] Such a conformational change is unique to S100 proteins because the exiting helix (helix 4 of EF2) is typically held in place via an X-type four-helix bundle that composes the tight dimer interface, whereas in other EF-hand-containing proteins, the exiting helix is free to rotate.

In general, proteins in the S100 family are distributed in a cell-specific manner and interact with a diverse set of molecules.[5–7] For S100A1, at least 20 known protein targets have been identified, including Ca^{2+}-signaling proteins (ryanodine receptors 1 and 2, Serca2a, and phospholamban), neurotransmitter

*Corresponding author. E-mail address: dweber@umaryland.edu.

Abbreviations used: GFAP, glial fibrillary acidic protein; NOE, nuclear Overhauser enhancement; 2D, two-dimensional; NOESY, NOE spectroscopy; TOCSY, total correlated spectroscopy; RDC, residual dipolar coupling; Pnt, pentamidine; TAMRA, carboxytetramethylrhodamine; NDR, nuclear Dpf2-related.

release proteins (synapsins I and II), cytoskeletal and filament-associated proteins [CapZ, microtubules, intermediate filaments, tau, microfilaments, desmin, tubulin, F-actin, titin, and the glial fibrillary acidic protein (GFAP)], transcription factors and their regulators (myoDand p53), enzymes (aldolase, phosphoglucomutase, malate dehydrogenase, glycogen phosphorylase, photoreceptor guanyl cyclases, adenylate cyclases, glyceraldehyde-3-phosphate dehydrogenase, twitchin kinase, nuclear Dpf2-related (NDR) kinase, and F1 ATP synthase), and other Ca^{2+}-activated proteins (annexins V and VI, S100B, S100A4, S100P, and other S100 proteins) (reviewed in Refs. 6 and 7). It is also the case that several S100 protein family members bind to the same protein target.[6,7] For example, both S100A1 and S100B, two of the earliest discovered S100 proteins, interact in a Ca^{2+}-dependent manner with several of the same protein targets including the ryanodine receptor, microtubules, GFAP, p53, NDR kinase, phosphoglucomutase, CacyBP/Sip1, and annexin A6;[6,8–13] hence, it is possible that some S100 proteins may function redundantly. Furthermore, using phage display techniques, Ivanenkov *et al.* identified a 12-amino-acid peptide (TRTKIDWNKILS) derived from the actin-capping protein (CapZ) that bound to S100B in a Ca^{2+}-dependent manner at low micromolar concentrations.[14] Subsequently, S100A1 and several other S100 proteins (i.e., S100A1, S100A4, and S100A5) have also been shown to bind this same peptide, termed TRTK12 (Wright, N. T. & Weber, D. J., unpublished data).[5] As a result, the TRTK12 peptide is considered a general S100 protein consensus binding sequence [(K/R)(L/I)XWXXIL].

To examine in detail how two S100 proteins can bind to the same protein target, we have determined the solution structure of S100A1–TRTK12 and compared it to the previously determined structure of S100B–TRTK12.[15] NMR chemical shift perturbation data were suggestive that TRTK12 interacts with the hydrophobic pocket that is common to both Ca^{2+}-S100A1 and Ca^{2+}-S100B.[4,5] However, when these two structures were compared here at atomic resolution, it was found that the specific positioning of the TRTK12 peptide in the target binding pocket was not conserved in S100A1 and S100B and that interactions between the peptide and the two S100 protein side chains were considerably different. This structure also leads to salient insights into the necessary attributes of productive S100A1–target protein interactions, some of which may be common in several S100–target protein interactions, including those for S100B.

Results

Chemical shift and NOE assignments for the S100A1–TRTK12 complex

The first step in solving the high-resolution structure of S100A1–TRTK12 (24 kDa) by NMR was to unambiguously assign the resonances and nuclear Overhauser enhancement (NOE) correlations for the complex, using data from a series of heteronuclear multidimensional NMR experiments. The ^{1}H, ^{13}C, and ^{15}N chemical shift assignments for all observable backbone and side-chain resonances of ^{13}C,^{15}N-labeled S100A1 bound to TRTK12 were completed *a priori* using standard NMR through-bond experiments as described in Wright *et al.*[5] Unambiguous resonance and NOE assignments for protons of the unlabeled TRTK12 peptide bound to ^{13}C,^{15}N-labeled S100A1 were then made using two-dimensional (2D) ^{12}C-filtered spectra [NOE spectroscopy (NOESY) and total correlated spectroscopy (TOCSY) in H_2O and D_2O], as previously described for other protein–peptide complexes.[15–18] Representative NOE data from a region of a 2D ^{12}C-filtered NOESY collected in D_2O is illustrated (Fig. 1a), which show NOE correlations for bound TRTK12 between $I10_{\delta}$ and other protons of I10 ($I10_{\alpha}$ and $I10_{\gamma 2}$) as well as to protons of K9 ($K9_{\beta,\gamma,\delta}$) and W7 ($W7_{\delta,\xi}$). That W7 was proximal to I10 also provided an early indication that the TRTK12 peptide was helical when bound to Ca^{2+}-S100A1 (Fig. 1a). In addition, proton resonances for I10 and W7 of TRTK12 (i.e., $I10_{\gamma 2}$, $I10_{\delta}$, and $W7_{\delta,\xi}$) were found to be proximal to the β-protons of C85 of ^{13}C,^{15}N-labeled S100B in a 3D ^{13}C-edited, ^{12}C-filtered NOESY experiment (Fig. 1b). Intermolecular NOE data such as these were critically important for the structure determination of the S100A1–TRTK12 complex as well as for validating proton assignments on unlabeled TRTK12 bound to S100A1 (Fig. 1b). In summary, the observable ^{1}H resonances of TRTK12 together with the ^{1}H, ^{13}C, and ^{15}N resonances of S100A1 in the S100A1–TRTK12 complex were assigned unambiguously and deposited into the BioMagResBank (BMRB) database† under BMRB accession number 16050.

NOE assignments were made using data from 3D ^{15}N-edited NOESY, 3D ^{13}C-edited NOESY, 4D ^{15}N,^{13}C-edited NOESY, and 4D ^{13}C,^{13}C-edited NOESY experiments (Fig. 1c). As found in all other dimeric S100 protein structures, it was clear from NOE data that helices 1 and 4 were an integral part of the S100A1 dimer interface in the S100A1–TRTK12 complex.[19] For example, early in the NOE assignment and structure determination process, several NOE correlations were observed between residues at the N- and C-termini of helix 1 (i.e., $L4_{\delta 1}$ to $F15_{HN}$ and several others). Because of the physical impossibility of having two residues at opposite ends of a helix being proximal in space, such NOE correlations were assigned as intersubunit between helices 1 and 1′ of the S100A1 dimer. Similarly, the assignment of intermolecular NOEs could be made for residues at the N- and C-termini of helices 4 and 4′ due to the antiparallel alignment of these helices (i.e., $F71H_N$ to $V83_{g1}$, and several others). As expected, such NOE data for S100A1 in the S100A1–TRTK12 complex were fully consistent

† http://www.bmrb.wisc.edu

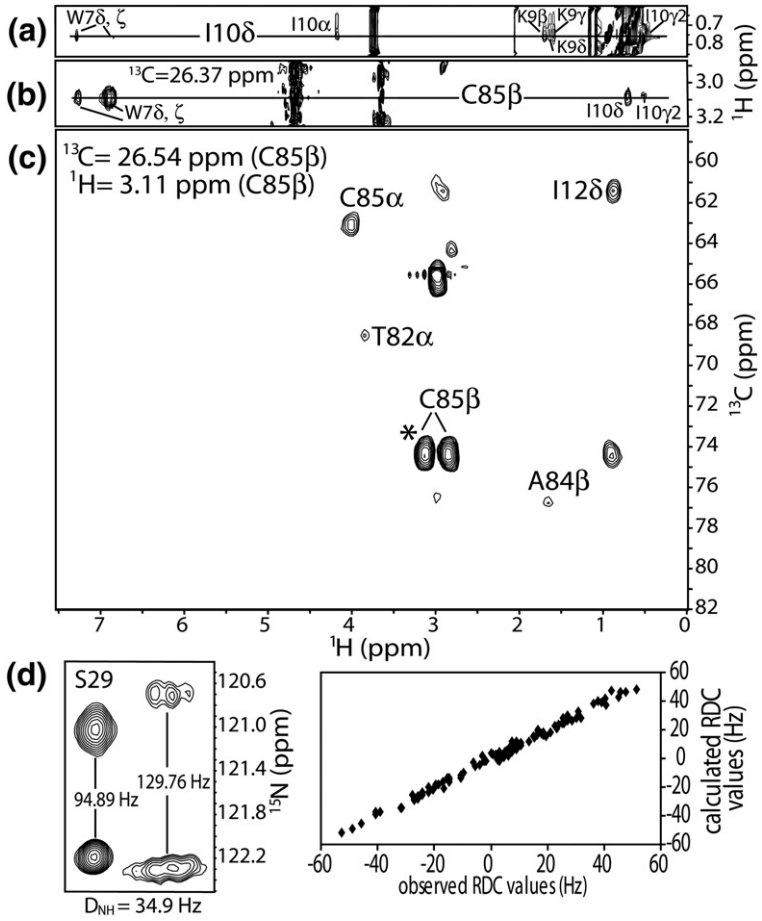

Fig. 1. NOE data used to determine the structure of Ca^{2+}-S100A1 bound to TRTK12 at 37 °C, pH 7.2. (a) Region of the ^{12}C-filtered NOESY experiment, showing NOE correlations between protons of Trp7 and Lys9 to Ile10$_\delta$ of TRTK12 when bound to Ca^{2+}-S100A1. These NOE correlations are not present in spectra of samples containing the TRTK12 peptide alone. (b) Strip of the 3D ^{13}C-edited, ^{12}C-filtered NOESY spectrum, demonstrating NOE correlations between C85$_\beta$ of S100A1 to several protons of both Trp7 and Ile10 of TRTK12. (c) Plane of the 4D ^{13}C,^{13}C-edited NOESY showing medium- and long-range NOE correlations from C85$_\beta$ of S100A1. Each of these spectra was collected on samples containing ^{13}C,^{15}N-labeled S100A1 and unlabeled TRTK12 peptide. (d) RDC data from the amide of S29 in isotropic (left) and aligned (right) media, illustrating typical N–H$_N$ splittings. On the right, a plot of expected RDCs *versus* observed RDCs, showing that the data fit well into structure calculations.

with the antiparallel alignment of helices 1, 1′, 4, and 4′ into an X-type four-helix bundle at the dimer interface as found for other S100 proteins. It was then relatively straightforward to continue assigning both intra- and intersubunit NOE correlations in an iterative manner with preliminary structural models as a guide. For example, a NOE correlation observed between the H$^\beta$ protons of C85 and H$^\delta$ protons of I12 (Fig. 1c) was assigned as an intermolecular NOE since these two protons were more than 20 Å apart within the same subunit. In total, 130 intermolecular NOE constraints were assigned unambiguously at the dimer interface for residues in helix 1 (E3, L4, E5, T6, A7, M8, T10, L11, I12, V14, and F15), loop 2 or "hinge" (E40 and L41), and helix 4 (F71, F74, V75, V76, A80, T82, V83, and C85). An additional 38 NOE correlations remained ambiguous and were allowed to satisfy inter- and/or intramolecular distance constraints even in the final structure calculation (Table 1), as previously described for other symmetric dimers.[20]

Next, the structure and positioning of the TRTK12 peptide in the S100A1–TRTK12 complex were examined in detail. Important for these analyses was a 3D ^{13}C-edited, ^{12}C-filtered NOESY experiment, which provided 96 intermolecular protein–peptide distance constraints between ^{13}C,^{15}N-labeled S100A1 and unlabeled TRTK12 peptide (Fig. 1b). For example, W7, I10, and L11 of TRTK12 exhibited intermolecular NOE correlations to C85 on S100A1. In general, these three hydrophobic residues of TRTK12 provided a large number of NOE correlations to hydrophobic residues in helix 4. This periodicity of recurring intermolecular NOE correlations, combined with (i, i+3) intrapeptide NOE correlations from the ^{12}C-filtered NOESY experiment (Fig. 1a), allowed for the precise orientation of TRTK12 into the hydrophobic binding site in Ca^{2+}-S100A1 and further confirmed that TRTK12 folds as a helix when bound to S100A1. As was also found for the S100B–TRTK12 complex, all five residues defining the S100A1/S100B consensus binding sequence of TRTK12 peptide [(K/R)(L/I)XWXXIL] including K4, I5, W7, I10, and L11 were found to be at the S100A1–TRTK12 binding interface.[14] In total, protons from 8 residues of the TRTK12 peptide (K4, I5, W7, N8, K9, I10, L11, and S12) gave intermolecular NOE correlations to protons from 14 residues on S100A1 (F44, L45, K49, D50, D52, A53, K56, I57, E60, L77, L81, A84, C85, and F88), consistent with the helical TRTK12 peptide oriented nearly parallel with helix 3 on S100A1, spanning from the hinge region (loop 2) to the middle of helices 3 and 4.

Residual dipolar coupling measurements

In an effort to improve and independently verify the NOE-based structure, we measured N–H$_N$ and C$^\alpha$–H$^\alpha$ residual dipolar coupling (RDC) data with the use of a radially compressed polyacrylamide gel

Table 1. NMR-derived restraints and statistics of 20 NMR structures[a]

	⟨20⟩	Best
RMSD from distance constraints (Å)[b]		
Total (3382)	0.037±0.002	0.036
Intraresidue (570)	0.009±0.004	0.010
Sequential ($\|i-j\|=1$) (962)	0.029±0.003	0.028
Medium range ($1<\|i-j\|\leq 1$) (848)	0.036±0.003	0.035
Long range ($\|i-j\|>5$) (446)	0.045±0.005	0.045
Intermolecular for dimer interface (130)	0.044±0.006	0.034
Ambiguous intra- or inter-S100A1 subunit (38)	0.012±0.010	0.005
TRTK12 peptide (sequential, medium) (90)	0.028±0.009	0.041
Intermolecular S100A1 to TRTK12 peptide (96)	0.060±0.011	0.062
Calcium ligand (18)	0.025±0.010	0.029
Hydrogen bonds (184)	0.069±0.005	0.064
RMSD from experimental dihedral constraints (°)		
Φ,Ψ (276)	0.516±0.120	0.502
RMSD from dipolar coupling restraints (Hz)		
D_{N-H} (112)	1.652±0.093	1.606
D_{C-H} (136)	3.296±0.171	3.261
RMSD from experimental ^{13}C chemical shifts (ppm)		
$^{13}C^{\alpha}$	1.261±0.041	1.253
$^{13}C^{\beta}$	1.054±0.039	1.020
RMSD from idealized geometry		
Bonds (Å)	0.006±0.001	0.006
Angles (°)	0.978±0.018	0.959
Impropers (°)	1.841±0.010	1.844
Lennard–Jones potential energy (kcal/mol)[c]	−889±28	−917
Q-factor[d]	0.26±0.04	0.25
Percentage of residues in the most favorable region of the Ramachandran plot[e]	87.6±2.4	91.3
RMSD to the mean structure (Å)[f]		
All backbone atoms in S100A1 (3–88)	0.518±0.088	0.339
All heavy atoms in S100A1 (3–88)	1.097±0.128	0.943
All ordered backbone (S100A1 3–88, TRTK12 4–12)	0.565±0.089	0.476
All heavy atoms (S100A1 3–88, TRTK12 4–12)	1.118±0.118	0.969

[a] The 20 ensemble structures, ⟨20⟩, are the results of simulated annealing calculations. The best structure is that closest to the average structure. The values shown for the ⟨20⟩ are the means±standard deviations.

[b] All four subunits of the protein complex are included in all of these values. None of the 20 structures has a distance violation >0.4 Å or a dihedral angle violation of >5°. The force constants used in the simulated annealing calculations are as follows: 1000 kcal mol^{-1} $Å^{-2}$ for bond length, 500 kcal mol^{-1} rad^{-2} for angles and improper torsions, 4 kcal mol^{-1} $Å^{-4}$ for the quartic van der Waals repulsion term [hard-sphere effective van der Waals set to 0.8 times their values in CHARMM (Chemistry at Harvard Macromolecular Mechanics) parameters], 50 kcal mol^{-1} $Å^{-2}$ for experimental distance constraints, 100 kcal mol^{-1} $Å^{-2}$ for noncrystallographic symmetry, 1 kcal mol^{-1} $Å^{-2}$ for distance symmetry constraints, 0.5 kcal mol^{-1} ppm^{-2} for the ^{13}C chemical shift constraints, and 1.0 for the conformational database potential. The force constants (in kcal Hz^{-2}) used for dipolar coupling restraints were as follows: 0.40 for ^{15}N–$^{1}H_N$ and 0.2 for $^{13}C^{\alpha}$–$^{1}H^{\alpha}$.

[c] Lennard–Jones van der Waals energies were calculated using CHARMM parameters and were not used in any stage of the structure determination.

[d] *Q*-factors were determined by randomly removing 10% of all RDC values. An ensemble of structures with a second randomly removed subset of RDCs was also run to ensure accuracy. The *Q*-factor of this second set was 0.26.

[e] PROCHECK was utilized to generate the Ramachandran plot.

[f] Backbone calculations include C^{α}, N, and C′ atoms. Only residues 3–88 are included since no long-range NOE correlations were observed for residues 1–2 and 89–93 in S100A1 or residues 1–3 in the TRTK peptide.

to partially align the protein (Fig. 1d), as previously described.[21] In the absence of decoupling, the observed splitting between two nuclei P and Q corresponds to the sum of the scalar and dipolar interactions, J_{PQ} and D_{PQ}. J_{PQ} is independent of alignment, and D_{PQ} is simply obtained from the difference between the P–Q splitting measured in conditions where the sample is partially aligned (i.e., in radially compressed gels) *versus* conditions with isotropic tumbling.[22] Here, 112 $^{1}D_{N-H}$ values for S100A1 in the S100A1–TRTK12 complex were recorded from a ^{15}N–^{1}H 2D correlation spectrum in the absence of ^{1}H decoupling during the t_1 evolution period, and the upfield and downfield components of the ^{15}N–$\{^{1}H_N\}$ doublets were separated into two spectra in an interleaved manner as described previously[22] (Fig. 1d). Additionally, $^{1}D_{C\alpha\text{-}H\alpha}$ dipolar couplings were obtained under the same alignment conditions as those for $^{1}D_{N-H}$ RDCs. These data were collected using a 3D (H)CA(CO)NH experiment recorded in the absence of ^{1}H decoupling during the C^{α} evolution period, permitting accurate measurement of 136 $^{1}D_{C\alpha\text{-}H\alpha}$ RDCs, as described previously.[23] Because the $^{1}D_{N-H}$ and $^{1}D_{C\alpha\text{-}H\alpha}$ data were collected under identical alignment conditions, they could be fit simultaneously in structure calculations to enforce a single alignment tensor ($A_a \sim 0.6\times10^{-3}$).

Structure calculations, structural statistics, and description of the S100A1–TRTK12 complex solved in solution by NMR spectroscopy

In total, 3382 experimental distance constraints, 276 dihedral angle constraints, and 248 RDC constraints were used to calculate the solution structure of the

dimeric Ca^{2+}-S100A1–TRTK12 complex (>18 constraints per residue) (Fig. 2). The first three residues of the TRTK12 peptide showed no intermolecular NOE correlations, while the last nine residues showed more than 10 NOE correlations per residue on average. The large number of assigned NOE correlations allowed for an accurate residue-by-residue examination of the S100A1–TRTK12 binding interface, although the N-terminal tail of TRTK12 remains undefined and likely is dynamic in solution. A family of the 20 lowest-energy structures of S100A1–TRTK12 is depicted in stereo view in Fig. 2a. These structures all have low *Q* factors (0.26), no dihedral violations greater than 5°, no NOE violations greater than 0.4 Å, and no residues in the unfavorable portion of the Ramachandran plot (Table 1). The backbone atoms in each of the 20 structures are well-defined with an RMSD of 0.57 for all ordered residues and an RMSD of 0.52 for just the S100A1 backbone alone (Table 1). For the bound TRTK12 peptide, the backbone is slightly less well defined, with an RMSD of 0.81 for all ordered residues. No long-range NOE correlations were observed for residues 1–2 and 89–93 in Ca^{2+}-S100A1 or for residues 1–3 of the TRTK12 peptide, and thus, these were removed from RMSD calculations (Table 1).

Overall, the backbone atoms of S100A1 do not significantly deviate in position between the Ca^{2+}-bound state and the peptide-bound state, with the RMSD for C^{α} carbons between the two states being 1.31 Å (Tables 2 and 3). This maintenance of the classical S100 fold upon target protein binding was also observed when TRTK12 bound to Ca^{2+}-S100B as well as when a peptide derived from the ryanodine receptor (RyRP12) bound to Ca^{2+}-S100A1 (Tables 2 and 3); thus, the S100A1 structure reported here is likely a conserved feature of Ca^{2+}-dependent S100A1–target protein interactions. In the absence of S100A1, the TRTK12 peptide exists as a random coil, as judged by a lack of NOE correlations and a narrow range of NMR spectral data.[15] However, when bound to Ca^{2+}-S100A1, the C-terminal region of TRTK12 adopts a helical conformation, as judged by both characteristically α-helical interpeptide

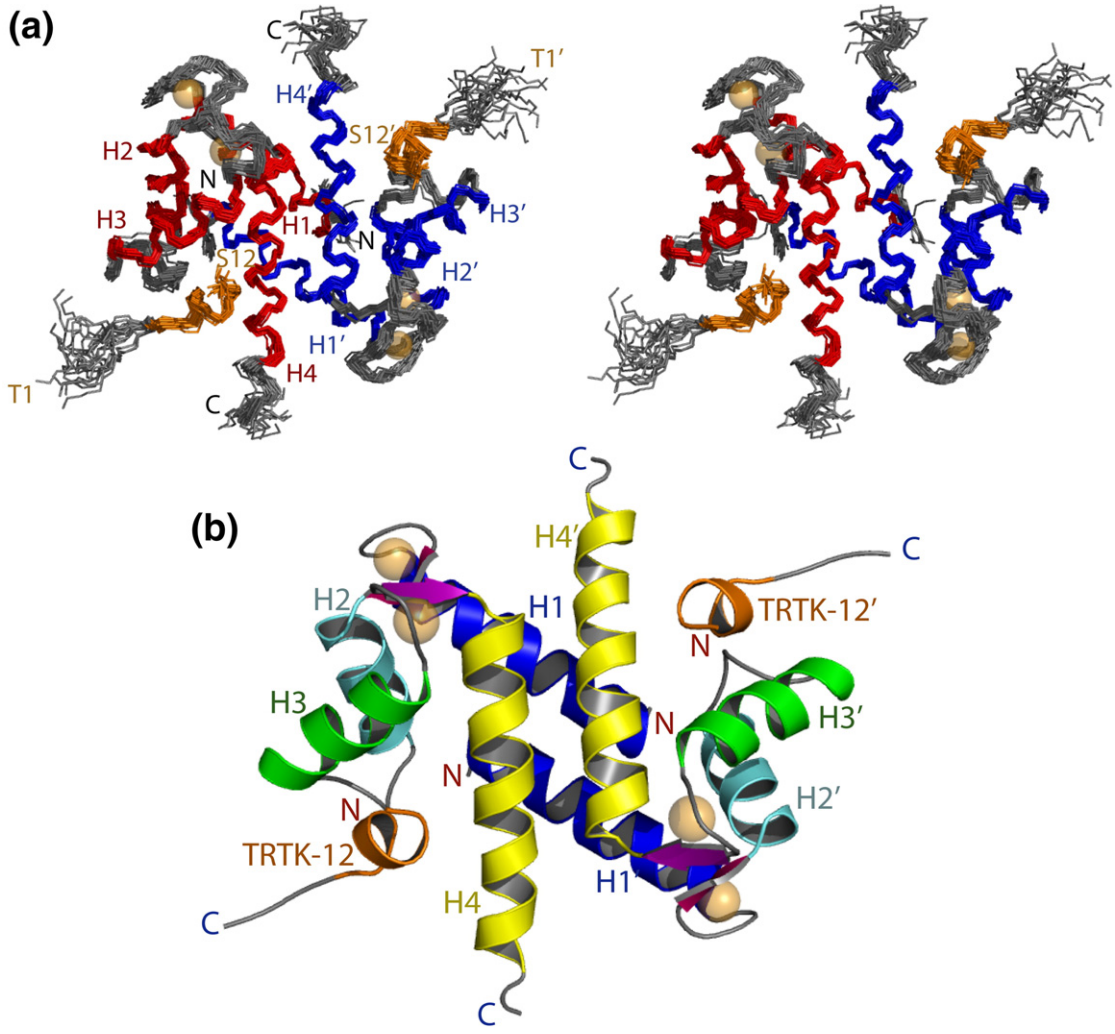

Fig. 2. The 3D structure of the S100A1–TRTK12 complex. (a) Stereo view of the 20 lowest-energy structures with the RMSD for backbone atoms found to be 0.672 (residues 3–87 of S100A1 and residues 4–12 of TRTK12). The two subunits are colored red and blue for S100A1, respectively, and the TRTK12 peptide is colored orange. (b) Ribbon diagram illustrating the fold of the S100A1–TRTK12 complex.

Table 2. Interhelical angles of S100A1 and S100B complexes

Helices[a]	Apo-S100A1[b]	Ca^{2+}-S100A1[c]	S100A1–Ca^{2+}-RyRP12[d]	S100A1–Ca^{2+}-TRTK12	Ca^{2+}-S100B[e]	S100B–Ca^{2+}-TRTK12[f]
I–II	120±3	132±1	136±2	131±1	137±5	132±2
I–III	−45±2	−102±2	−94±2	−106±2	−118±5	−118±3
I–IV	107±2	131±2	125±2	126±2	128±4	128±1
II–III	148±2	125±2	126±1	121±2	104±3	109±2
II–IV	46±1	−29±1	−35±2	−37±2	−35±4	−33±2
III–IV	−150±1	121±2	136±2	120±2	106±4	108±4
I–I′	−165±3	−157±3	−153±2	−155±2	−155±1	−148±2
IV–IV′	176±2	152±3	156±2	156±2	159±5	146±3
I–peptide	—	—	88±7	−106±4	—	−63±11
II–peptide	—	—	−49±7	103±3	—	164±11
III–peptide	—	—	−163±4	38±2	—	55±11
IV–peptide	—	—	49±7	127±4	—	143±7

[a] Interhelical angles (Ω) range from −180° to 180° and are classified as either parallel (||) for 0° |Ω| 40° and 140° |Ω| 180° or perpendicular (⊥) for 40° |Ω| 140° as described.[24]
[b] Taken from the NMR structure (PDB code 1K2H).[25]
[c] Taken from the NMR structure (PDB code 1ZFS).[5]
[d] Taken from the NMR structure (PDB code 2J2K).[17]
[e] Taken from the NMR structure (PDB code 1QLK).[4]
[f] Taken from the NMR structure (PDB code 1MWN).[15]

NOEs (Fig. 1a) and intrasubunit NOE correlations (Figs. 1b and 3a). Interestingly, the observation that S100A1 interacts with helical portions of target proteins is another feature that is observed in nearly all of the S100–target protein structures reported thus far and is likely another general feature for S100–target protein interactions.

The Ca^{2+} dependence of the S100A1–TRTK12 interaction

Upon the addition of Ca^{2+} to dimeric apo-S100A1, helix 3 of both subunits reorients by ~90° relative to helix 4.[5] As a consequence of this conformational change, a hydrophobic pocket defined by amino acid residues in the hinge (loop 2; F44 and L45), helix 3 (I57), and helix 4 (L77, L81, A84, C85, and F88), which were buried in the apo-state, is exposed when Ca^{2+} binds to S100A1 (Fig. 3). These same residues form multiple contacts with W7, I10, and L11 of TRTK12 (Fig. 3). The most prominent TRTK12 side chain involved in an interaction with S100A1 is the large hydrophobic side chain of W7, which extends into a well-formed hydrophobic groove formed by residues F44, L45, L81, A84, C85, and F88 of Ca^{2+}-S100A1. Additionally, ring stacking between F88 and F44 on S100A1 and W7 on TRTK12 is observed, which is consistent with experiments in which S100A1 is truncated at F88 and binding to TRTK12 is abrogated.[8] The hydrophobic residues I10 and L11 of TRTK12 also interact with numerous hydrophobic residues on helix 3 and helix 4 of S100A1 and are peripherally associated with the deep W7 binding pocket, as judged by a large number of NOE correlations to S100A1 between these residues and hydrophobic residues in the S100A1 binding pocket (Fig. 3). Thus, it is concluded that TRTK12 forms an amphipathic helix and that substantial hydrophobic interactions, most notably those between W7 on TRTK12 and a series of residues on S100A1, serve to stabilize the S100A1–TRTK12 complex.

The TRTK12–S100A1 interaction, driven by the formation of an interprotein hydrophobic binding site, stabilizes the canonical EF-hand of S100A1 (EF2). This is experimentally manifested through an increase in the Ca^{2+}-binding affinity of S100A1 in the presence of peptide (Fig. 4). Here, Tb^{3+} binding and kickoff experiments were performed with S100A1 in the presence of TRTK12, as previously described.[5] Changes in Tb^{3+} luminescence intensity were measured upon binding to the tight site (EF2) of S100A1 ($^{Tb}K_d = 149 \pm 3$ nM; Fig. 4, inset), and Ca^{2+} binding to S100A1 was then determined in direct competition studies with Tb^{3+}. As observed in Fig. 4, S100A1 binds Ca^{2+} at 8±3 μM in the presence of

Table 3. EF-hand angles of S100 proteins based on the VGM method

EF-hand	N-terminal coordinate of second helix	θ (°)	ϕ (°)
Pseudo-EF-hand			
S100A1–Ca^{2+}-TRTK12[a]	(8.659, 2.341, −5.416)	53±2	80±3
S100A1–Ca^{2+}-RyRP12[b]	(9.236, −1.916, −5.779)	45±2	84±5
Ca^{2+}-S100A1[c]	(9.237, −2.133, −4.516)	51±2	82±2
Ca^{2+}-S100B–TRTK12[d]	(0.927, −0.838, −7.262)	55±2	95±3
Ca^{2+}-S100B[e]	(11.199, −3.856, −6.578)	53±4	79±5
Apo-S100A1[f]	(11.843, −4.311, −5.724)	68±4	85±9
Typical EF-hand			
S100A1–Ca^{2+}-TRTK12[a]	(9.191, 2.880, −4.310)	60±2	115±5
S100A1–Ca^{2+}-RyRP12[b]	(9.919, 1.444, 5.583)	45±2	83±2
Ca^{2+}-S100A1[c]	(8.928, −2.392, −3.789)	58±2	108±3
Ca^{2+}-S100B–TRTK12[d]	(9.070, −1.009, −5.863)	70±4	112±3
Ca^{2+}-S100B[e]	(9.073, −2.602, −6.819)	76±5	95±7
Apo-S100A1[f]	(5.246, 13.667, −0.067)	35±2	−90±7

[a] Vector geometry mapping results were obtained using the program VGM as described.[24] Apo-calmodulin of Zhang *et al.* (PDB code 1DMO) was used as the reference for these calculations as previously described.[26]
[b] Taken from the NMR structure (PDB code 2J2K).[17]
[c] Taken from the NMR structure (PDB code 1ZFS).[5]
[d] Taken from the NMR structure (PDB code 1MWN).[15]
[e] Taken from the NMR structure (PDB code 1QLK).[4]
[f] Taken from the NMR structure (PDB code 1K2H).[25]

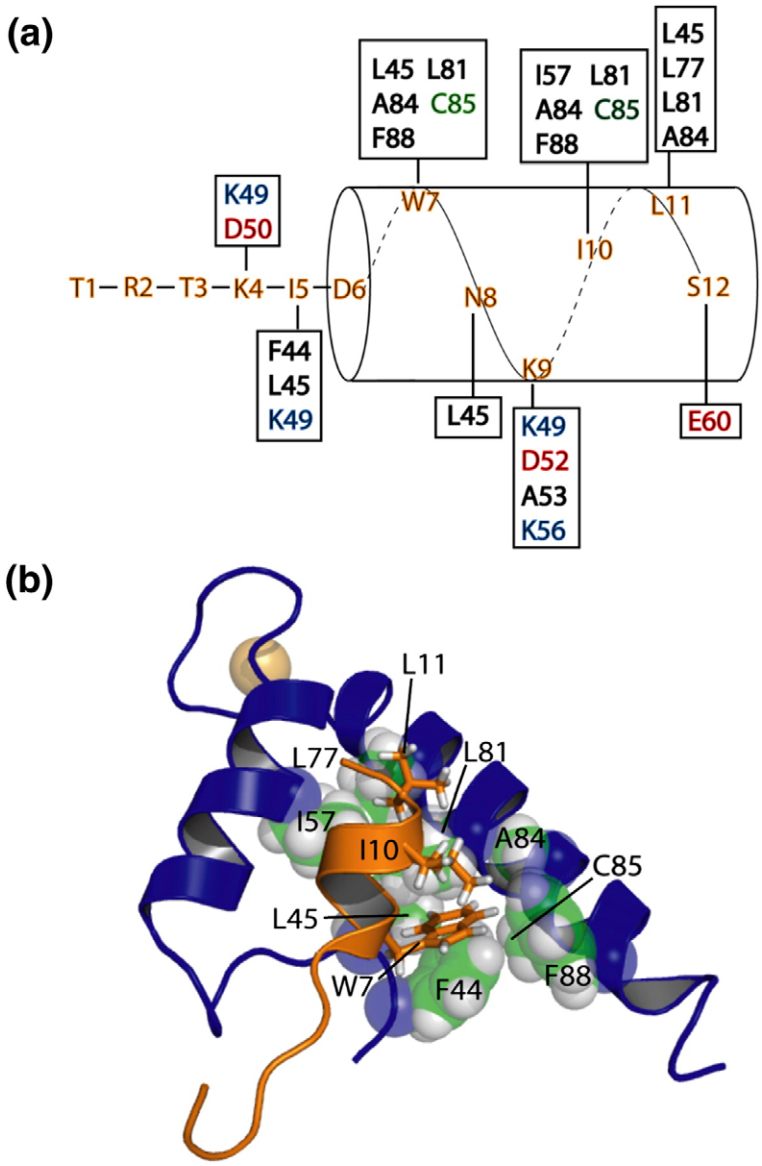

Fig. 3. Hydrophobic residues of TRTK12 interact with a hydrophobic binding pocket on Ca^{2+}-S100A1. (a) Residues that give intermolecular NOE correlations between the TRTK12 peptide and residues on S100A1 (in boxes) are illustrated. S100A1 residues are colored black for hydrophobic, green for polar, red for negatively charged, and blue for positively charged residues. (b) Residues of TRTK12 including W7, I10, and L11 are packed nearby hydrophobic residues from the hinge region (F44and L45), helix 3 (I57), and helix 4 (L77, L81, A84, C85, and F88) of S100A1. In particular, W7 fits into a well-formed hydrophobic pocket consisting of F44, L45, L81, A84, C85, and F88 of Ca^{2+}-S100A1.

TRTK12, which is more than threefold tighter than when no peptide is present (27 μM). Such an increase in the Ca^{2+} affinity is well documented among S100 proteins and other EF-hand-containing proteins in general when target proteins are bound.[27–34]

The drug pentamidine inhibits S100A1–TRTK12 complex formation

There is a growing interest in developing inhibitors of S100A1 because they could be beneficial in treating a variety of human diseases including neurological diseases, diabetes mellitus, heart failure, and several types of cancer.[35–38] The absence of significant phenotypes in S100A1 knockout mice suggests that an S100A1 antagonist would have minimal side effects in normal tissues.[39,40] In the brain, increased S100A1 expression contributes to pathologies related to neurological diseases, which suggests that S100A1 inhibitors could reverse such processes. For example, neuronal PC12 cells that do not express S100A1 are more resistant to Aβ-induced cell death than cells that express normal levels of S100A1,[35] indicating that S100A1 antagonists would be beneficial in treating Alzheimer's disease. In addition, extracellular S100A1 is cytotoxic to PC12 cells[41,42] and injection of anti-S100A1 antibodies were found to lessen learning and memory deficits.[43] Other S100A1-regulated intracellular processes are also consistent with S100A1 augmentation of Alzheimer's disease pathology. These include S100A1-linked altered APP expression, destabilization of Ca^{2+} homeostasis, S100A1-mediated increased cell growth, decreased dendritic arborization, and decreased tubulin polymerization/stability.[35,44]

As previously found for S100B, the U.S. Food and Drug Administration-approved drug pentamidine (Pnt) has been found to bind S100A1 and block its interaction with TRTK12. Specifically, a fluorescently labeled carboxytetramethylrhodamine (TAMRA)–

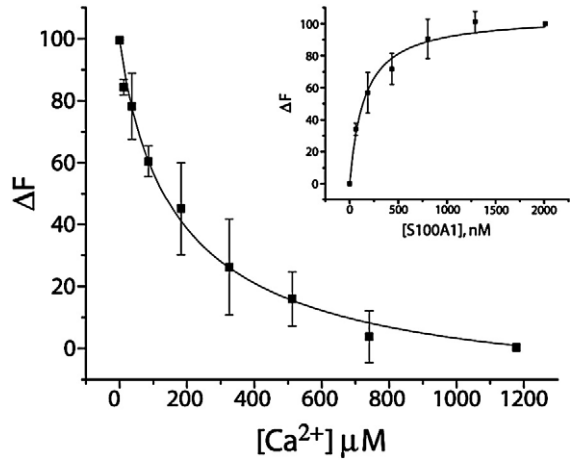

Fig. 4. Ca^{2+} and Tb^{3+} binding to S100A1–TRTK12 as monitored via Tb^{3+} luminescence. Displacement of Tb^{3+} by Ca^{2+} from a Tb^{3+}-S100A1–TRTK12 complex as monitored by the decrease in Tb^{3+} luminescence. The sample conditions included 50 μM TRTK12, 20 mM Hepes buffer, pH 7.0, and 20 mM DTT at 25 °C in D_2O. The $^{Ca}K_d$ calculated from this competition experiment ($^{Ca}K_d = 8 \pm 3$ μM) relied on the dissociation of Tb^{3+} from the Tb^{3+}-S100A1–TRTK12 complex in the same buffer ($^{Tb}K_d = 149 \pm 3$ nM; inset). In this titration (inset), S100A1 was titrated into a solution where [Tb^{3+}] was kept constant (3 μM) and [TRTK12] was kept at a concentration (50 μM) where Tb^{3+}-S100A1 is fully saturated with TRTK12 peptide at all points in the titration.

TRTK peptide was found to bind ($K_d = 1.0 \pm 0.6$ μM) to Ca^{2+}-S100A1 (Fig. 5, inset). This affinity of TAMRA–TRTK12 is ~20-fold tighter than that of unlabeled TRTK12 ($K_d = 23 \pm 6$ μM), which is likely due to additional interactions between the protein and the hydrophobic TAMRA moiety. Furthermore, increasing amounts of Pnt were sufficiently able to displace the TAMRA-labeled peptide from Ca^{2+}-S100A1, as judged by a decrease in fluorescence anisotropy values (Fig. 5). With the use of the equations employed by Nikolovska-Coleska *et al.*,[45] the calculated K_d of Pnt for S100A1 is 130 ± 60 μM (as compared to a K_d of 39 ± 5 μM for the S100B–Pnt complex)[46] and provides evidence that Pnt is a potential lead compound for developing S100A1 inhibitors. These competitive binding data also indicate that Pnt binds to S100A1 in the TAMRA–TRTK12 binding pocket and could represent a starting point for developing drugs that block S100A1 through at least partial occlusion of this site. This may eventually lead to the development of novel high-affinity molecules that specifically inhibit S100A1 and can be tested *in vivo*.

Discussion

S100A1 and S100B, two of the earliest S100 proteins discovered, have been reported to bind the ryanodine receptor, microtubules, GFAP, p53 (also binds S100A2 and S100A4), NDR kinase, phosphoglucomutase, CacyBP/Sip1 (also binds S100A6 and S100A12), and annexin A6 (also binds S100A6) (reviewed in Refs. 7 and 17; Wright, N. T. & Weber, D. J., unpublished results). Likewise, other target proteins have also been shown to bind multiple S100 proteins including annexin A5 (S100A1, S100A6, and S100A12), caldesmon (S100A1 and S100A6), and Sgt1 (S100A6 and S100P). The completion of this structure represents a chance to study in detail how two S100 proteins, S100A1 and S100B, interact with the same peptide, TRTK12.[15] Specifically, both S100A1 and S100B bind to TRTK12 at micromolar concentrations (S100B, $K_d = 7 \pm 1$ μM;[6] S100A1, $K_d = 23 \pm 6$ μM), and upon comparison of chemical shift perturbation data, TRTK12 was thought to be oriented in a similar manner relative to helix 3 and helix 4 in the S100B–TRTK12 and S100A1–TRTK12 complexes.[5] However, a comparison of the two NMR structures shows side-chain interactions that stabilize the peptide–protein interface differ substantially between S100A1 and S100B (Fig. 6a and b), which could provide an explanation for the approximately threefold difference in affinity observed. Specifically, W7 in TRTK12 does not extend close to helix 3 in Ca^{2+}-S100A1, as observed in Ca^{2+}-S100B, but instead is located near another hydrophobic pocket close to the C-terminus of S100A1 (Figs. 3b and 6a and b). This change in tryptophan position for TRTK12 has the consequence of rotating the entire peptide so that the hydrophobic

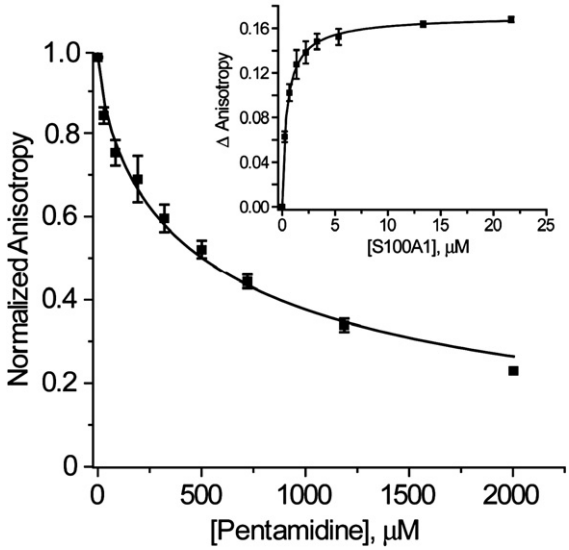

Fig. 5. Pnt binding to Ca^{2+}-S100A1. Displacement of TAMRA-labeled TRTK12 bound to Ca^{2+}-S100A1 by the U.S. Food and Drug Administration-approved drug Pnt as monitored by a decrease in TAMRA–TRTK12 fluorescence anisotropy. The sample conditions included 3.5 μM S100A1, 50 nM TAMRA-labeled TRTK12, 25 mM NaCl, 1.0 mM $CaCl_2$, 1 mM DTT, and 5 mM Hepes buffer, pH 7.5, at 25 °C. The $^{Pnt}K_d$ calculated from this competition experiment ($^{Pnt}K_d = 120 \pm 60$ μM) relied on the dissociation of TAMRA-labeled TRTK12 from Ca^{2+}-S100A1 ($^{TAMRA-TRTK}K_d = 1.0 \pm 0.6$ μM; inset). In this titration (inset), S100A1 was titrated into a solution where [TAMRA–TRTK] was kept constant (50 nM), with all other buffer conditions the same as in the competition experiment.

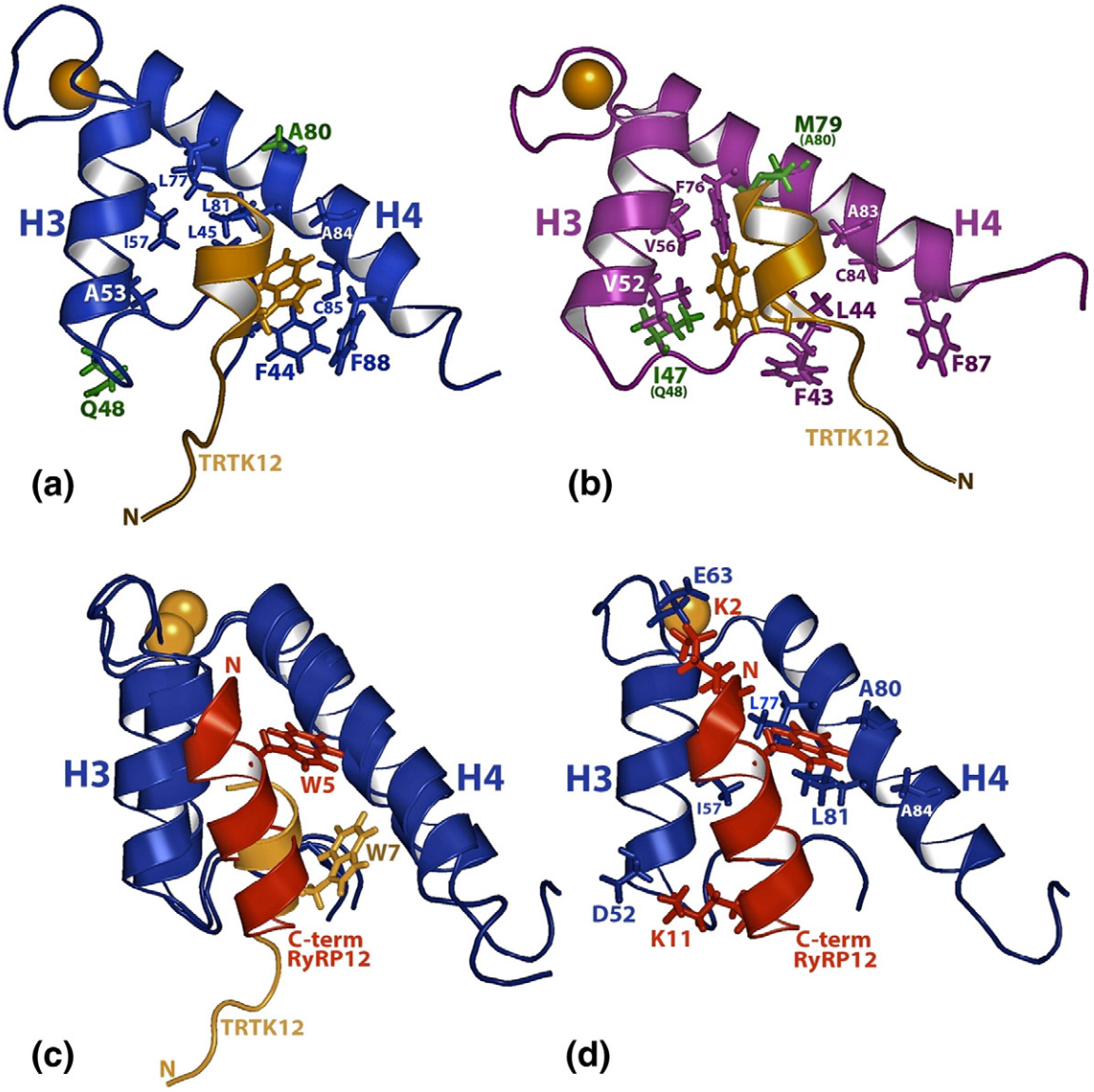

Fig. 6. Comparison of the S100B–TRTK12, S100A1–RyRP12, and S100A1–TRTK12 structures. (a) Ribbon diagram illustrating TRTK12 (tan) bound to Ca^{2+}-S100A1 (blue). Residues that are not similar between the S100A1 and S100B sequences are shown in green. (b) Ribbon diagram illustrating TRTK12 (tan) bound to Ca^{2+}-S100B (purple). As in (a), residues that are very dissimilar between the S100A1 and S100B sequences are shown in green. (c) Overlay of ribbon diagrams of TRTK12 (tan) and RyRP12 (red) bound to Ca^{2+}-S100A1 (blue). In this panel, the location of the tryptophan residue in each peptide (W5 for RyRP12; W7 for TRTK12) is illustrated. (d) Ribbon diagram illustrating RyRP12 (red) bound to Ca^{2+}-S100A1 (blue) illustrating the side chains of S100A1 that interact with the RyRP12 peptide.

face of the helical peptide faces helix 4 of S100A1 more directly than it does helix 4 of S100B. Specifically, the hydrophobic tryptophan residue of TRTK12 interacts with a binding pocket in S100A1 that comprises residues from loop 2, termed the hinge (F44 and L45), and helix 4 (L81, A84, C85, and F88). Comparatively, different residues in S100B from the hinge (I47), helix 3 (V52, V56), and helix 4 interact with W7 on TRTK12 (Fig. 6b). That this pocket is different on S100A1 *versus* S100B is likely the result of differences in protein sequence, most notably the nonconservative changes of an isoleucine (I47 in S100B) for a glutamine (Q48 in S100A1) and a methionine (M79 in S100B) for an alanine (A80 in S100A1; Fig. 6a and b, residues colored green). Another more subtle change in the sequences is a valine residue (V52 in S100B) for an alanine residue (A53 in S100A1). These and other differences in sequence result in a deep hydrophobic tryptophan-binding site in S100B nearby helix 3, which does not exist in S100A1. That S100A1 can form a different hydrophobic tryptophan-binding pocket adjacent to helix 4 is also likely facilitated by the fact that S100A1 has an alanine residue at position 80 rather than a methionine (i.e., M79). This allows W7 of TRTK12 to more readily approach the other large hydrophobic residues (i.e., F44, L45, L81, and F88) that compose the S100A1 TRTK12 binding site (Fig. 6).

Our laboratory recently published a structure of S100A1 bound to a peptide, RyRP12, derived from ryanodine receptor (KKAVWHKLLSKQ).[17,39] Like TRTK12, this peptide closely resembles the consensus binding sequence of S100 proteins. However, the peptide-binding sites on Ca^{2+}-S100A1 were found to be quite different when the NMR structures of these two complexes were compared (Fig. 6c and d). For example, both RyRP12 and TRTK12 form amphipathic helices and bind a hydrophobic binding site exposed in Ca^{2+}-S100A1, but the two peptides were oriented differently in the pocket by nearly 180°. For example, RyRP12 aligns parallel with helix 4 of S100A1, with the tryptophan residue on this peptide (W5) located in a hydrophobic binding pocket slightly higher in the Ca^{2+}-S100A1 binding pocket than that of the tryptophan residue (W7) of TRTK12 (Fig. 6c). Furthermore, in RyRP12, W5 is stabilized by different residues in helix 3 (I57) and helix 4 (L77, A80, and L81) than W7 in TRTK12, which interacts with residues in the hinge (F44 and L45) and helix 4 (L81, A84, C85, and F88). Examination of residue-by-residue contacts between both complexes also reveals that the RyRP12 and TRTK12 peptides interact with S100A1 via leucine/isoleucine residues (I10 and L11 in TRTK12 and L8 and L9 in RyRP12) in addition to the aromatic tryptophan residue. However, unlike what is found in the S100A1–TRTK12 complex, two lysine residues in RyRP12 (K2 and K11) likely form electrostatic interactions with S100A1 (E63 and D52 in S100A1), which could contribute to the orientation of RyRP12 in the S100A1 binding site.[47] The TRTK12 peptide has no such electrostatic interactions with S100A1 and is oriented in the hydrophobic pocket based on van der Waals and hydrophobic interactions alone. From these two structures, it appears likely that there is no one preferred orientation of binding for S100A1 targets and that each S100A1 binding partner may orient differently using different key residues in the hydrophobic pockets nearby helices 3 and 4 and the hinge.

Examination of other S100–target peptide complexes reveals that while tryptophan is frequently used in S100–target interactions, other residues can substitute; in both the S100A11–annexin 1 complex and the S100A6–Siah 1 structure, tryptophan is replaced with leucine.[48,49] Such variability in a residue position that has been assumed to be fairly well conserved among S100 binding motifs suggests that other previously unsuspected sequences could be high-affinity targets to various members of the S100 family. That S100 proteins can bind to more than one target (i.e., K_d of S100A1 for TRTK12 = 23 ± 6 μM, while the K_d for RyRP12 = 8 μM)[39,50] and that different S100 proteins can bind to the same target suggest that many S100 proteins interact with their targets via the "selected fit" mechanism of binding. With the use of this model, Ca^{2+}-S100A1 exists as an ensemble of equilibrium structures, with the protein binding pocket sampling multiple similar but not identical conformations. Productive S100A1–target complex formation occurs when S100A1 attains the conformation(s) most compatible for that particular target protein.[51] Thus, unique targets can select for particular conformations, leading to a diverse set of potential interactions. Evidence supporting this hypothesis is seen in Ca^{2+}-S100B, where regions that compose the target binding pocket experience both fast and slow time scale dynamics.[52] This mechanism of binding may be a common feature in the S100 family of proteins, since most S100 proteins are reported to bind multiple protein targets.

Conclusions

Here, we present the solution structure of Ca^{2+}-S100A1 bound to the 12-residue peptide TRTK12, which comprises an exact match of the S100 consensus binding sequence. A comparison of the apo-, Ca^{2+}-, and Ca^{2+}-S100A1–TRTK12 structures clearly reveals why this interaction is Ca^{2+} dependent. TRTK12 binds S100A1 as an amphipathic helix, with its hydrophobic face in close contact with the hydrophobic binding pocket of S100A1. Close examination of this interaction reveals that several residues, most notably W7 on the TRTK12 peptide, are fully buried in a well-formed hydrophobic cleft on S100A1. TRTK12 is uniquely oriented in the S100A1 binding site, as compared to the similar peptide RyRP12. Additionally, both S100B and S100A1 bind TRTK12 differently. A detailed examination of the S100A1 and S100B structures furthers our understanding of how these similar proteins interact with their respective target molecules and elicit distinct cellular functions. This information in turn forms the underpinning for specific rational drug-design efforts toward inhibiting one or both of these S100 proteins when they are elevated in a disease state.

Materials and Methods

Sample preparations

A synthetic peptide (ac-TRTKIDWNKILS-am) derived from the α subunit of CapZ (residues 267–276) was chemically synthesized with its N-terminus acetylated (-ac) and C-terminus amidated (-am) and prepared for NMR as described previously.[10] The TAMRA–TRTK peptide is synthesized with the TAMRA fluorescent covalently labeled at the N-terminus with the C-terminus amidated (-am). Recombinant ^{15}N- and ^{13}C,^{15}N-labeled rat S100A1 protein (10.5 kDa per subunit) was purified after overexpression in *Escherichia coli* [HMS174(DE3)] as described.[5] NMR samples contained 15 mM d_{11}-Tris–HCl, pH 7.2, 15 mM DTT, 10 mM $CaCl_2$, 0.34 mM NaN_3, 20 mM NaCl, 10% ^2H_2O, TRTK12 peptide (2–6 mM), and S100A1 (1–3 mM; subunit concentration). The acrylamide solutions used in the dipolar coupling experiments were prepared fresh at 30% acrylamide (1:20 bis) concentration. Compressed gels contained 5% acrylamide solution, 0.015% *N*,*N*,*N*′,*N*′-tetramethylethylenediamine, and 0.015% ammonium persulfate and were prepared as previously described.[5]

NMR spectroscopy

NMR spectra were collected at 37 °C with a Bruker DMX600 NMR spectrometer (600.13 MHz for protons) and a Bruker AVANCE 800 NMR spectrometer (800.27 MHz for protons) each equipped with four frequency channels and 5-mm triple-resonance *z*-axis gradient cryogenic probeheads. Sequential backbone and side-chain assignments of S100A1 in the TRTK12 peptide complex were obtained using standard NMR spectroscopy methods as described.[5] The sequential assignments for the unlabeled TRTK12 peptide bound to ^{13}C,^{15}N-labeled Ca^{2+}-S100A1 were based on correlations recorded in ^{12}C-filtered TOCSY and ^{12}C-filtered NOESY experiments.[53–55] The filtered TOCSY spinlock time (75 ms) and the filtered NOESY mixing time (200 ms) were sufficient for the collection of high-quality proton NMR data for TRTK12 in a protein complex of this molecular mass (24.2 kDa).[15,18] 4D ^{13}C,^{15}N-edited NOESY–heteronuclear single-quantum coherence (HSQC)[56] and 4D ^{13}C,^{13}C-edited NOESY–HSQC spectra, both with a mixing time of 130 ms, were collected on a sample containing ^{13}C,^{15}N S100A1 bound to unlabeled TRTK12. A 3D ^{12}C-filtered, ^{13}C-edited NOESY with a mixing time of 200 ms was also collected for recording intermolecular NOE correlations at the peptide–protein interface, as previously described.[15,39]

Structure calculation

Interproton distance constraints were derived from 2D, 3D, and 4D NOESY experiments (2D NOESY, ^{12}C-filtered 2D NOESY; ^{15}N-edited 3D NOESY; ^{12}C-filtered, ^{13}C-edited 3D NOESY; ^{15}N, ^{13}C-edited 4D NOESY; and ^{13}C,^{13}C-edited 4D NOESY) as described previously.[5] Dihedral constraints $\phi\pm20$ and $\psi\pm15°$ for α-helix and $\phi\pm40$ and $\psi\pm40°$ for β-sheet were included based on $^{3}J^{\alpha}_{NH-H}$ coupling constants, hydrogen-exchange rates, and the chemical shift index of $^{1}H^{\alpha}$ and $^{13}C^{\alpha}$ resonances. Distance constraints of 2.0–2.8 Å between Ca^{2+} and protein ligands were included based on the EF-hand model for a typical and S100-type Ca^{2+}-binding domain, respectively. An ensemble of structures, calculated without these Ca^{2+} restraints, had an RMSD of 0.625, demonstrating that the inclusion of such restraints had no effect on the overall structure of the complex. Hydrogen-bond constraints of $r_{HN-O}=1.5–2.8$ Å and $r_{N-O}=2.4–2.5$ Å were included in the final stage of structure calculations. Structures calculated without hydrogen bonds had an RMSD of 0.653 when compared with those calculated with hydrogen bonds, indicating that inclusion of these constraints also had little or no influence on the overall structure. Pseudopotentials for secondary $^{13}C^{\alpha}$ and $^{13}C^{\beta}$ chemical shifts and a conformational database potential were included in the final simulated annealing refinements with the computer program Xplor.[24] The internuclear dipolar coupling (in hertz) was determined from the difference in *J* splitting between isotropic and radially compressed polyacrylamide-aligned phases with both a 2D IPAP ^{1}H–^{15}N HSQC to record N–H_N splittings and a 3D (H)CA(CO)NH experiment without H^{α} decoupling during C^{α} acquisition in t_2 to record C^{α}–H^{α} splittings and was incorporated into the final structure calculation as previously described.[5,17] *Q*-factors were calculated by randomly removing ~10% of both the N–H_N and C^{α}–H^{α} RDC data and then comparing these values to those back-calculated from the structure. The final 20 structures were selected (from 200) based on lowest energy and were of high quality based on the statistical criteria listed in Table 1.

Luminescence spectroscopy

All experiments used to determine binding constants were performed on an Aminco-Bowman Series 2 luminescence spectrophotofluorometer with a temperature probe (quartz cuvette) maintained at 25 °C. The binding constants were obtained from titrations, repeated in triplicate, and performed with at least two different concentrations of Tb^{3+}. Typical conditions for S100A1 titrations included 20 mM Hepes buffer, pH 7.0, and 20 mM DTT, 100 mM TRTK12, and 1–5 mM Tb^{3+}. These samples were lyophilized and resuspended in the appropriate volume of D_2O. Competition experiments, repeated in triplicate, used the same sample as the Tb^{3+} binding experiments, with the addition of 1–5 mM S100A1. Ca^{2+} K_d values were calculated using $K_d = K'/(1+[Tb^{3+}]/{}^{Tb}K_d$, where K' is from the best-fit curve of the Ca^{2+} titration data and the ${}^{Tb}K_d$ term is from the best-fit curve of the Tb^{3+} titration data.

Fluorescence anisotropy

All experiments were performed using fluorescence spectroscopy techniques on an SLM-Aminco Bowman Series 2 (Thermo, Asheville, NC) fluorescence spectrophotometer with an excitation wavelength of 542 nm and an emission wavelength of 590 nm. All experiments were repeated three or more times, and all samples were studied at 25 °C with sample conditions consisting of 5 mM Hepes, pH 7.5, 1 mM DTT, 25 mM NaCl, 1 mM $CaCl_2$, and 50 nM TRTK12–TAMRA. Fluorescence anisotropy measurements during Pnt competition binding studies were used to monitor the binding of TRTK–TAMRA to S100A1 using the same set of conditions with the addition of 3.5 mM S100A1. The binding data were fit using a single-site binding model with Origin software (OriginLab Corp., Northampton, MA) and one peptide and one Pnt molecule bound per S100A1 subunit. An equation derived by Nikolovska-Coleska *et al.* was used for determination of the K_d, as previously described, using:[45]

$$K_d = [I]_{50}/([L]_{50}/{}^{TAMRA-TRTK}K_d + [P]_0/{}^{TAMRA-TRTK}K_d + 1) \quad (1)$$

where $[I]_{50}$ is the concentration of Pnt at 50% inhibition, $[L]_{50}$ is the concentration of the free TAMRA–TRTK peptide at 50% inhibition, $[P]_0$ is the concentration of the free protein at 0% inhibition, and ${}^{TAMRA-TRTK}K_d$ is the dissociation constant of S100A1–TAMRA–TRTK12.

Accession numbers

Coordinates and structure factors for the S100A1–TRTK12 complex have been deposited in the Protein Data Bank (PDB) with accession number 2kbm, and chemical shift assignments for the S100A1–TRTK12 complex have been deposited in the BMRB (accession number 16050).

Acknowledgements

This work was supported by grants from the National Institutes of Health (GM58888 and CA107331 to D.J.W.). The NMR spectrometers used

in these studies were purchased, in part, with funds from shared instrumentation grants from the National Institutes of Health (S10 RR10441, S10 RR15741, and S10 RR16812; S10 RR23447 to D.J.W.) and from the National Science Foundation (DBI 0115795 to D.J.W.). N.T.W. was partially supported by National Institute of Arthritis and Musculoskeletal and Skin Diseases training grant T32 AR007592 to the Interdisciplinary Program in Muscle Biology, University of Maryland School of Medicine, and by an American Heart Association training grant (0615343U). We would also like to thank Thomas Charpentier for his assistance in editing the manuscript and for helping to prepare figures.

References

1. Strynadka, N. C. J. & James, M. N. G. (1989). Crystal structures of the helix–loop–helix calcium-binding proteins. *Annu. Rev. Biochem.* **58**, 951–998.
2. Ikura, M. & Yap, K. L. (2000). Where cancer meets calcium—p53 crosstalk with EF-hands. *Nat. Struct. Biol.* **7**, 525–527.
3. Smith, S. P. & Shaw, G. S. (1998). A novel calcium-sensitive switch revealed by the structure of human S100B in the calcium-bound form. *Structure*, **6**, 211–222.
4. Drohat, A. C., Baldisseri, D. M., Rustandi, R. R. & Weber, D. J. (1998). Solution structure of calcium-bound rat S100B(betabeta) as determined by nuclear magnetic resonance spectroscopy. *Biochemistry*, **37**, 2729–2740.
5. Wright, N. T., Varney, K. M., Ellis, K. C., Markowitz, J., Gitti, R. K., Zimmer, D. B. & Weber, D. J. (2005). The three-dimensional solution structure of Ca(2+)-bound S100A1 as determined by NMR spectroscopy. *J. Mol. Biol.* **353**, 410–426.
6. Wilder, P. T., Lin, J., Bair, C. L., Charpentier, T. H., Yang, D., Liriano, M. *et al.* (2006). Recognition of the tumor suppressor protein p53 and other protein targets by the calcium-binding protein S100B. *Biochim. Biophys. Acta*, **1763**, 1284–1297.
7. Santamaria-Kisiel, L., Rintala-Dempsey, A. C. & Shaw, G. S. (2006). Calcium-dependent and -independent interactions of the S100 protein family. *Biochem. J.* **296**, 201–214.
8. Garbuglia, M., Verzini, M., Rustandi, R. R., Osterloh, D., Weber, D. J., Gerke, V. & Donato, R. (1999). Role of the C-terminal extension in the interaction of S100A1 with GFAP, tubulin, the S100A1- and S100B-inhibitory peptide, TRTK-12, and a peptide derived from p53, and the S100A1 inhibitory effect on GFAP polymerization. *Biochem. Biophys. Res. Commun.* **254**, 36–41.
9. Garbuglia, M., Verzini, M. & Donato, R. (1998). Annexin VI binds S100A1 and S100B and blocks the ability of S100A1 and S100B to inhibit desmin and GFAP assemblies into intermediate filaments. *Cell Calcium*, **24**, 177–191.
10. Rustandi, R. R., Baldisseri, D. M., Drohat, A. C. & Weber, D. J. (1999). Structural changes in the C-terminus of Ca^{2+}-bound rat S100B (beta beta) upon binding to a peptide derived from the C-terminal regulatory domain of p53. *Protein Sci.* **8**, 1743–1751.
11. Landar, A., Caddell, G., Chessher, J. & Zimmer, D. B. (1996). Identification of an S100A1/S100B target protein: phosphoglucomutase. *Cell Calcium*, **20**, 279–285.
12. Arcuri, C., Giambanco, I., Bianchi, R. & Donato, R. (2002). Annexin V, annexin VI, S100A1 and S100B in developing and adult avian skeletal muscles. *Neuroscience*, **109**, 371–388.
13. Filipek, A., Jastrzebska, B., Nowotny, M. & Kuznicki, J. (2002). CacyBP/SIP, a calcyclin and Siah-1-interacting protein, binds EF-hand proteins of the S100 family. *J. Biol. Chem.* **277**, 28848–28852.
14. Ivanenkov, V. V., Jamieson, G. A., Jr, Gruenstein, E. & Dimlich, R. V. (1995). Characterization of S-100b binding epitopes. Identification of a novel target, the actin capping protein, CapZ. *J. Biol. Chem.* **270**, 14651–14658.
15. Inman, K. G., Yang, R., Rustandi, R. R., Miller, K. E., Baldisseri, D. M. & Weber, D. J. (2002). Solution NMR structure of S100B bound to the high-affinity target peptide TRTK-12. *J. Mol. Biol.* **324**, 1003–1014.
16. Osawa, M., Tokumitsu, H., Swindells, M. B., Kurihara, H., Orita, M., Shibanuma, T. *et al.* (1999). A novel target recognition revealed by calmodulin in complex with Ca^{2+}-calmodulin-dependent kinase kinase. *Nat. Struct. Biol.* **6**, 819–824.
17. Wright, N. T., Prosser, B. L., Varney, K. M., Zimmer, D. B., Schneider, M. F. & Weber, D. J. (2008). S100A1 and calmodulin compete for the same binding site on ryanodine receptor. *J. Biol. Chem.* **283**, 26676–26683.
18. Rustandi, R. R., Baldisseri, D. M. & Weber, D. J. (2000). Structure of the negative regulatory domain of p53 bound to S100B(betabeta). *Nat. Struct. Biol.* **7**, 570–574.
19. Weber, D. J., Rustandi, R. R., Carrier, F. & Zimmer, D. B. (2000). The molecular basis of calcium action in biology and medicine. In *Interaction of Dimeric S100B (ββ) with the Tumor Suppressor Protein: A Model for Ca-ependent S100–Target Protein Interactions* (Pochet, R., ed), pp. 469–487, Kluwer Academic Publishers, Dordrecht, the Netherlands.
20. Nilges, M. (1993). A calculation strategy for the structure determination of symmetric dimers by ^{1}H NMR. *Proteins*, **17**, 297–309.
21. Lipsitz, R. S. & Tjandra, N. (2004). Residual dipolar couplings in NMR structure analysis. *Annu. Rev. Biophys. Biomol. Struct.* **33**, 387–413.
22. Ottiger, M., Delaglio, F. & Bax, A. (1998). Measurement of J and dipolar couplings from simplified two-dimensional NMR spectra. *J. Magn. Reson.* **131**, 373–378.
23. Tjandra, N., Omichinski, J. G., Gronenborn, A. M., Clore, G. M. & Bax, A. (1997). Use of dipolar ^{1}H–^{15}N and ^{1}H–^{13}C couplings in the structure determination of magnetically oriented macromolecules in solution. *Nat. Struct. Biol.* **4**, 732–738.
24. Schwieters, C. D., Kuszewski, J. J., Tjandra, N. & Clore, G. M. (2003). The Xplor-NIH NMR molecular structure determination package. *J. Magn. Reson.* **160**, 65–73.
25. Rustandi, R. R., Baldisseri, D. B., Inman, K. G., Nizner, P., Hamilton, S. H., Landar, A. *et al.* (2002). Three-dimensional solution structure of the calcium-signaling protein apo-S100A1 as determined by NMR. *Biochemistry*, **41**, 788–796.
26. Zhang, M., Tanaka, T. & Ikura, M. (1995). Calcium-induced conformational transition revealed by the solution structure of apo calmodulin. *Nat. Struct. Biol.* **2**, 758–767.
27. Markowitz, J., Rustandi, R. R., Varney, K. M., Wilder, P. T., Udan, R., Wu, S. L. *et al.* (2005). Calcium-binding properties of wild-type and EF-hand mutants of S100B in the presence and absence of a peptide derived from the C-terminal negative regulatory domain of p53. *Biochemistry*, **44**, 7305–7314.
28. Johnson, J. D., Snyder, C., Walsh, M. & Flynn, M. (1996). Effects of myosin light chain kinase and peptides on Ca^{2+} exchange with the N- and C-terminal Ca^{2+} binding sites of calmodulin. *J. Biol. Chem.* **271**, 761–767.

29. Olwin, B. B., Edelman, A. M., Krebs, E. G. & Storm, D. R. (1984). Quantitation of energy coupling between Ca^{2+}, calmodulin, skeletal muscle myosin light chain kinase, and kinase substrates. *J. Biol. Chem.* **259**, 10949–10955.
30. Persechini, A., White, H. D. & Gansz, K. J. (1996). Different mechanisms for Ca^{2+} dissociation from complexes of calmodulin with nitric oxide synthase or myosin light chain kinase. *J. Biol. Chem.* **271**, 62–67.
31. Yazawa, M., Vorherr, T., James, P., Carafoli, E. & Yagi, K. (1992). Binding of calcium by calmodulin: influence of the calmodulin binding domain of the plasma membrane calcium pump. *Biochemistry*, **31**, 3171–3176.
32. Durussel, I., Méhul, B., Bernard, D., Schmidt, R. & Cox, J. A. (2002). Cation- and peptide-binding properties of human calmodulin-like skin protein. *Biochemistry*, **41**, 5439–5448.
33. Stemmer, P. M. & Klee, C. B. (1994). Dual calcium ion regulation of calcineurin by calmodulin and calcineurin B. *Biochemistry*, **33**, 6859–6866.
34. Peersen, O. B., Madsen, T. S. & Falke, J. J. (1997). Intermolecular tuning of calmodulin by target peptides and proteins: differential effects on Ca^{2+} binding and implications for kinase activation. *Protein Sci.* **6**, 794–807.
35. Zimmer, D. B., Chaplin, J., Baldwin, A. & Rast, M. (2005). S100-mediated signal transduction in the nervous system and neurological diseases. *Cell. Mol. Biol. (Noisy-le-grand)*, **51**, 201–214.
36. Zimmer, D. B., Chessher, J., Wilson, G. L. & Zimmer, W. E. (1997). S100A1 and S100B expression and target proteins in type I diabetes. *Endocrinology*, **138**, 5176–5183.
37. Li, G., Barthelemy, A., Feng, G., Gentil-Perret, A., Peoc'h, M., Genin, C. & Tostain, J. (2007). S100A1: a powerful marker to differentiate chromophobe renal cell carcinoma from renal oncocytoma. *Histopathology*, **50**, 642–647.
38. Pelc, P., Vanmuylder, N., Lefranc, F., Heizmann, C. W., Hassid, S., Salmon, I. *et al.* (2003). Differential expression of S100 calcium-binding proteins in epidermoid cysts, branchial cysts, craniopharyngiomas and cholesteatomas. *Histopathology*, **42**, 387–394.
39. Prosser, B. L., Wright, N. T., Hernandez-Ochoa, E., Varney, K. M., Liu, Y., Olojo, R. O. *et al.* (2008). S100A1 binds to the calmodulin binding site of ryanodine receptor and modulates skeletal muscle EC coupling. *J. Biol. Chem.* **283**, 5046–5057.
40. Du, S. J., Cole, J. J., Tenis, N., Gao, X. M., Kontgen, F., Kemp, B. E. & Heierhorst, J. (2002). Impaired cardiac contractility response to hemodynamic stress in S100A1-deficient mice. *Mol. Cell. Biol.* **22**, 2821–2829.
41. Fulle, S., Mariggio, M. A., Belia, S., Petrelli, C., Ballarini, P., Guarnieri, S. & Fano, G. (1999). Rapid desensitization of PC12 cells stimulated with high concentrations of extracellular S100. *Neuroscience*, **89**, 991–997.
42. Mariggio, M. A., Fulle, S., Calissano, P., Nicoletti, I. & Fano, G. (1994). The brain protein S-100ab induces apoptosis in PC12 cells. *Neuroscience*, **60**, 29–35.
43. O'Dowd, B. S., Zhao, W. Q., Ng, K. T. & Robinson, S.R. (1997). Chicks injected with antisera to either S-100 alpha or S-100 beta protein develop amnesia for a passive avoidance task. *Neurobiol. Learn. Mem.* **67**, 197–206.
44. Zimmer, D. B., Cornwall, E. H., Reynolds, P. D. & Donald, C. M. (1998). S100A1 regulates neurite organization, tubulin levels, and proliferation in PC12 cells. *J. Biol. Chem.* **273**, 4705–4711.
45. Nikolovska-Coleska, Z., Wang, R., Fang, X., Pan, H., Tomita, Y., Li, P. *et al.* (2004). Development and optimization of a binding assay for the XIAP BIR3 domain using fluorescence polarization. *Anal. Biochem.* **332**, 261–273.
46. Charpentier, T. H., Wilder, P. T., Liriano, M. A., Varney, K. M., Pozharski, E., Mackerell, A. D., Jr *et al.* (2008). Divalent metal ion complexes of S100B in the absence and presence of pentamidine. *J. Mol. Biol.* **382**, 56–73.
47. Wright, N. T., Prosser, B. L., Varney, K. M., Zimmer, D. B., Schneider, M. F. & Weber, D. J. (2008). S100A1 and calmodulin compete for the same binding site on ryanodine receptor. *J. Biol. Chem.* **283**, 26676–26683.
48. Dempsey, A. C., Walsh, M. P. & Shaw, G. S. (2003). Unmasking the annexin I interaction from the structure of Apo-S100A11. *Structure*, **11**, 887–897.
49. Lee, Y. T., Dimitrova, Y. N., Schneider, G., Ridenour, W. B., Bhattacharya, S., Soss, S. E. *et al.* (2008). Structure of the S100A6 complex with a fragment from the C-terminal domain of Siah-1 interacting protein: a novel mode for S100 protein target recognition. *Biochemistry*, **47**, 10921–10932.
50. Wright, N. T., Margolis, J. W., Margolis, F. L. & Weber, D. J. (2005). Refinement of the solution structure of rat olfactory marker protein (OMP). *J. Biomol. NMR*, **33**, 63–68.
51. Wang, C., Karpowich, N., Hunt, J. F., Rance, M. & Palmer, A. G. (2004). Dynamics of ATP-binding cassette contribute to allosteric control, nucleotide binding and energy transduction in ABC transporters. *J. Mol. Biol.* **342**, 525–537.
52. Wright, N. T., Inman, K. G., Levine, J. A., Cannon, B. R., Varney, K. M. & Weber, D. J. (2008). Refinement of the solution structure and dynamic properties of Ca(2+)-bound rat S100B. *J. Biomol. NMR*, **42**, 279–286.
53. Ikura, M. & Bax, A. (1992). Isotope-filtered 2D NMR of a protein–peptide complex: study of a skeletal muscle myosin light chain kinase fragment bound to calmodulin. *J. Am. Chem. Soc.* **114**, 2433–2440.
54. Bax, A., Grzesiek, S., Gronenborn, A. M. & Clore, G. M. (1994). Isotope-filtered 2D HOHAHA spectroscopy of a peptide–protein complex using heteronuclear Hartmann–Hahn dephasing. *J. Magn. Reson., Ser. A*, **106**, 269–273.
55. Vuister, G. W., Kim, S. J., Orosz, A., Marquardt, J., Wu, C. & Bax, A. (1994). Solution structure of the DNA-binding domain of *Drosophila* heat shock transcription factor. *Nat. Struct. Biol.* **1**, 605–614.
56. Muhandiram, D. R., Guang, Y. X. & Kay, L. E. (1993). An enhanced-sensitivity pure absorption gradient 4D ^{15}N,^{13}C-edited NOESY experiment. *J. Biomol. NMR*, **3**, 463–470.